PHYSICAL REVIEW B VOLUME 51, NUMBER 10 1 MARCH 1995-II

Spatially resolved flux flow in long-overlap Josephson tunnel junctions

D. Quenter
Physikalisches Institut, Lehrstuhl Experimentalphysik II, Universität Tübingen, D-72076 Tübingen, Germany
and Physikalisch-Technische Bundesanstalt, Braunschweig, D-38116 Braunschweig, Germany

A. V. Ustinov
Institut für Schicht- und Ionentechnik, Forschungszentrum Jülich, D-52425 Jülich, Germany

S. G. Lachenmann, T. Doderer, and R. P. Huebener
Physikalisches Institut, Lehrstuhl Experimentalphysik II, Universität Tübingen, D-72076 Tübingen, Germany

F. Müller, J. Niemeyer, R. Pöpel, and T. Weimann
Physikalisch-Technische Bundesanstalt, Braunschweig, D-38116 Braunschweig, Germany

(Received 14 February 1994; revised manuscript received 31 August 1994)

Flux flow in different types of long-overlap Josephson junctions has been investigated by low-temperature scanning electron microscopy. The experimental results are compared with detailed numerical simulations. Describing the dynamics of the Josephson junction with the perturbed sine-Gordon equation, the flux-flow mode represents the case of high fluxon density in the junction. Due to the low damping in the investigated junctions (Nb/AlO$_x$/Nb and Nb/NbO$_x$/Pb based) a complicated interaction of the fluxon chain with reflected waves and cavity mode excitations occurred. The structure of these interactions was imaged with a spatial resolution of about 2 μm and investigated by the numerical simulations.

I. INTRODUCTION

Since the discovery of the Josephson effects in 1962,[1] the static and dynamic properties of Josephson tunnel junctions have been investigated extensively.[2,3] In addition to their basic physics, Josephson tunnel junctions are important for applications such as the voltage standard,[4,5] superconducting quantum interference devices (SQUID's),[6,7] superconductor-insulator-superconductor (SIS) mixers,[8] local oscillators,[9–13] and various digital devices.[13–15]

The dynamics of a distributed Josephson tunnel junction is described by the perturbed sine-Gordon equation (PSGE) together with appropriate boundary conditions.[15,16] Depending on the dimensions of the junction—in comparison with the Josephson penetration depth λ_J—and the applied magnetic field, different types of solutions of the PSGE can be found. In the dc current-voltage (I-V) characteristic these states manifest themselves by equally spaced current steps. The asymptotic step voltages are given by the formula

$$V_n = \frac{n\Phi_0\bar{c}}{2L}\,, \quad n = \pm 1, 2, 3, \dots \,. \tag{1}$$

Φ_0 is the magnetic flux quantum, $\bar{c}$ the phase velocity of electromagnetic waves in the junction (Swihart velocity), and L is the length of the junction.

In small tunnel junctions (i.e., a junction smaller than λ_J in both dimensions) with an applied magnetic field cavity-mode excitations, so-called Fiske steps (FS's), occur. The junctions act as an open-ended cavity and n [Eq. (1)] describes the mode order. For a long quasi-one-dimensional junction (length $L > \lambda_J$ and width $W < \lambda_J$) where no (or only a small) magnetic field is present, the resonant motion of Josephson vortices (fluxons) is possible, resulting in the zero-field steps (ZFS's) in the I-V curve. In this case n [Eq. (1)] takes only even values and $n/2$ is equal to the number of vortices inside the junction.

Increasing the applied magnetic field H [for $h > 2$, where $h \equiv H/(\lambda_J j_c)$ denotes the normalized magnetic field and j_c is the junction critical current density] multiple-fluxon states are possible and another kind of fluxon motion, the unidirectional flow of fluxons, occurs [Fig. 1(a)]. Under the influence of both the bias current I_B and the applied magnetic field H, the fluxons are created at one boundary of the junction, travel through the junction, and annihilate at the opposite boundary. In the dc I-V curve this kind of fluxon motion also appears as a current step [the so-called flux-flow step (FFS); see Figs. 1(b), 1(c)]. The asymptotic step voltage of the FFS is given by

$$V_{\mathrm{FFS}} = \frac{N_f\Phi_0\bar{c}}{L} = \Lambda H\bar{c}\,, \tag{2}$$

where $\Lambda = \lambda_L^{(1)} + \lambda_L^{(2)} + d$ is the magnetic field penetration depth perpendicular to the tunnel barrier of the junction ($\lambda_L^{(1)}$ and $\lambda_L^{(2)}$ denote the London penetration depths in the superconducting electrodes, and d is the thickness of the dielectric barrier) and N_f is the number of fluxons in the junction. In contrast to the resonant fluxon motion and to cavity-mode excitations the step V_{FFS} voltage no longer depends on the geometrical dimensions of the junction. In the flux-flow mode the asymptotic step voltage increases with the applied magnetic field. Qualitatively, we can understand the formation of the FFS due to an interaction of the oscillating Josephson current with the traveling electromagnetic wave—generated by the fluxons—of the same velocity inside the junction. Usually, due to the finite length of the junction, the I-V curve below the FFS consists of a series of smaller amplitude Fiske resonances at voltages given by Eq. (1) with $n \approx 2N_f$. These smaller steps appear as a consequence of cavity resonances excited by the small amplitude linear waves reflected from the boundaries.

The flux-flow mode of a long Josephson junction is an interesting regime displaying the dynamical properties of the system in the limit of high fluxon density. Recent applications of long junctions as local rf oscillators[11,12] for SIS mixers and, possibly, on-chip clocks have generated interest to get a better understanding of the flux-flow dynamics. In comparison with the resonant fluxon oscillator (based on the ZFS regime), the flux-flow oscillator offers several advantages. The position of the current step and therefore the oscillator frequency is not fixed by the geometrical dimensions of the junction and can be adjusted over a wide range by varying the applied magnetic field. The operation frequency of the flux-flow oscillator is substantially higher (up to 1.2 THz when using NbCN-based junctions[17]) and the emitted power ($\approx 10^{-6}$ W) is also about two orders of magnitude higher. One drawback of the flux-flow oscillator could be a relatively large linewidth of several hundred kHz.[10,11]

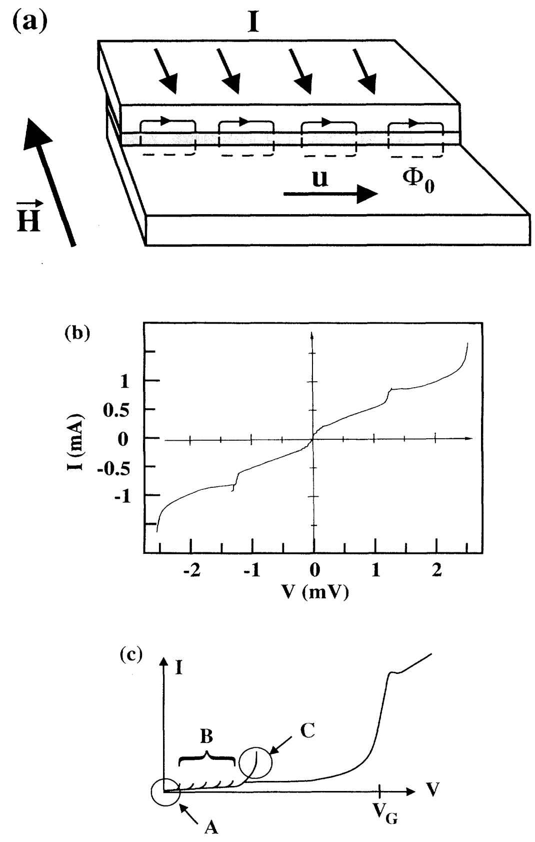

FIG. 1. Flux flow in overlap Josephon junctions. Part (a) shows a schematic drawing of a fluxon chain traveling through the junction with the speed u driven by the bias current I. $\vec{H}$ indicates the orientation of the applied magnetic field. Part (b) represents an experimental I-V curve in a Josephson junction of $L = 400$ μm with an external field of 0.81 mT. (c) shows a schematic I-V curve; A, B, and C indicate different regions of the flux-flow regime; V_G denotes the gap voltage.

Experimental studies of long Josephson tunnel junctions were mainly restricted to the integral properties such as the dc I-V curve and the emitted high-frequency radiation. Spatially resolved investigations either with electron beam[18–20] or laser beam scanning[21] allow one to study also local properties of the system. At the beginning of these spatially resolved investigations the static properties of distributed Josephson junctions have been examined. In the last few years the interest concentrated on various dynamic properties which have been studied using the technique of low-temperature scanning electron microscopy (LTSEM) or laser scanning.[22–31] The electron beam spot can act as a passive or an active probe. In the first case the dynamic state is not changed by scanning the sample with the electron beam spot. Alternatively, the beam is used as an active probe to modify the state of the junction—for example, by introducing new fluxons into the system. Mayer *et al.*[25] reported on a detailed investigation of one- and two-dimensional Fiske steps in square Josephson junctions. Here the electron beam acts as a passive probe. The most recent results using the electron beam as a passive probe dealt with a detailed investigation of the sine-Gordon dynamics in various junction geometries.[29] Electron beam scanning as an active probe was introduced by Ustinov *et al.*[26,27] In this case the electron beam served for injecting individual fluxons or Abrikosov vortices into a Josephson junction in order to change static or dynamic states of the junction.

While in former times detailed spatially resolved investigations of Fiske modes and the resonant fluxon motion were presented[25,29,31] we are going to present spatially resolved investigations of the flux-flow mode in Nb/AlO$_x$/Nb and Nb/NbO$_x$/Pb overlap Josephson tunnel junctions. The transition from the resonant case (such as ZFS's and FS's) to the unidirectional flux flow is one of the most complex issues of the long Josephson junction dynamics. The reason is that the dynamic flux-flow state involves a large number of fluxons moving in the junction strongly interacting with themselves and also with the quasilinear cavity waves excited due to the fluxon collision with the boundaries. The characteristic field where the transition to the flux-flow state takes place is close to the critical field H_{c1}, which is $h = 2$ in normalized units. For H close to H_{c1} the fluxon density is not very high and the internal degrees of freedom inside the fluxon chain can produce complicated dynamic states, which may be even a sort of intrinsic chaos. In this case the I-V characteristic often displays the so-called DLS (displaced linear slope; see Ref. 32) which has not been well understood (or even simulated numerically) until now. For these questions to be answered in line with the interaction between flux-flow and Fiske resonant modes in long junctions spatially resolving techniques are useful. Depending on the bias points and on the applied magnetic field we observed complicated interactions of the unidirectional fluxon motion and cavity-mode excitations. These results are compared with detailed numerical simulations.

In the following section we describe the experimental technique (Sec. II A) and present and discuss the results (Sec. II B) obtained by LTSEM. In Sec. III the theoretical model and the numerical technique will be described. These numerical results will be discussed and compared with the experimental ones. In Sec. IV a summary is given.

II. EXPERIMENT

A. Setup and technique

In the following we give a brief description of the experimental setup and technique; for details we refer to Ref. 33. We used a conventional scanning electron microscope, in which the standard sample holder is replaced by a liquid helium cryostat. The samples are fixed on a sapphire disk (which separates the liquid He from the vacuum inside the microscope) with a glue of high thermal conductance. The top of the sample can be scanned with the electron beam. To minimize incoming thermal radiation, the top of the sample holder is surrounded with a thermal radiation shield. An external magnetic field H can either be applied with superconducting coils which are mounted at the sample holder in the helium bath or with a magnetic control line placed directly on the chip. The whole sample holder is screened with a μ-metal shield to reduce the perturbations due to the external magnetic fields.

The main effect at the electron beam focus is a local heating of the sample around the beam position (x_0, y_0), the local temperature rise amounting to 0.1–10 K depending on the beam parameters. The spatial resolution of about 1–3 μm is determined by the thermal healing length η of the sample configuration. The beam power can be adjusted over a wide range to ensure that the electron beam acts only as a passive probe for the sample. In our case typically we used a beam power of about 0.25–2.5 μW with an acceleration voltage of 25 kV and a beam current of approximately 10–100 pA.

During the experiment we current biased the junction with a battery-powered current source. The voltage was filtered and amplified with a PAR 113 amplifier to record the dc I-V curve. In the current-biased junction the electron beam irradiation caused a voltage change $\Delta V(x_0, y_0)$ which was detected with a PAR 124 lock-in amplifier for an electron beam chopped with a frequency of 20 kHz. While scanning over the sample the beam-induced voltage change was simultaneously recorded with a digital imaging system (see Fig. 2). For these investigations we had to find an adequate signal generation model describing the junction response to the local perturbation. This will be done qualitatively in the next subsection together with the description of the experimental results. A quantitative model based on an numerical simulation will be discussed in Sec. III.

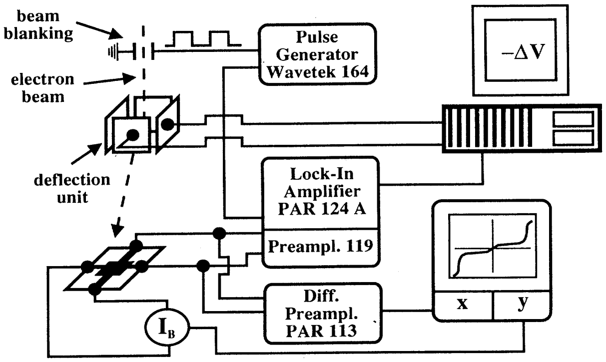

FIG. 2. Schematic of the experimental setup.

B. Results and discussion

During the experiments described below, the junctions were operated at the temperature $T \approx$ 4–6 K. The local temperature increase due to the electron beam irradiation was about 0.1–1 K . The relative magnitude of the voltage signal was $|\Delta V/V| \approx 10^{-4}$–$10^{-3}$, which indicates that the electron beam acts only as a small perturbation of the dynamic states in the Josephson junction. However, at some specific states or bias points we detected a higher-voltage signal, as will be described below.

We have investigated different types of Josephson junctions: Nb//AlO$_x$/Nb junctions with L=250 and 400 μm ($l = L/\lambda_J \approx$ 7.5–12) and a Nb/NbO$_x$/Pb junction with L =480 μm (l = 14). For all measured junctions the experimental data can be divided into three groups: (A) bias points close to $(I, V) \to (0, 0)$, (B) bias points at about a half of the FFS voltage, and (C) bias points at the FFS [see schematic I-V curve in Fig. 1 (c)].

First we discuss the results obtained at low bias current. Figures 3(a) and 3(b) show some examples of the imaging results. The images represent single line scans, obtained by scanning the electron beam along the junction length. The vertical axis displays the detected voltage signal $-\Delta V(x_0)$ in arbitrary units. The line scans show the periodically modulated distribution of the total dc Josephson current I_c due to the applied magnetic field. The number of periods is equal to the number of fluxons in the junction.

In previous studies[23,25–27,29] the signal generation for the dynamic states could be explained by a beam-induced change of the quasiparticle losses α and the surface losses β, whereas an influence of the change of the Josephson current density j_c was not significant. In contrast, for our experimental conditions on the low bias points [region A in Fig. 1(c)], where mainly static states are probed, the dominant effect of the electron beam heating is a change of the critical current I_c, whereas the change of the loss terms α and β can be ignored. The results are equivalent

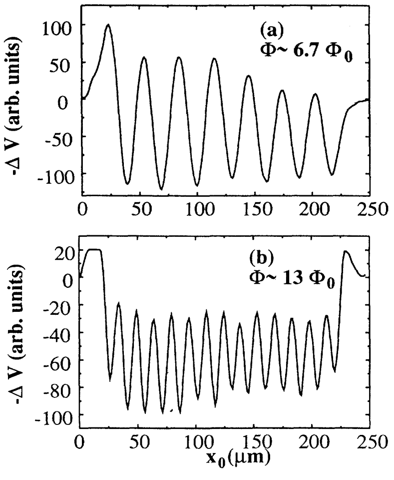

FIG. 3. Line scans $-\Delta V(x_0)$ of low-bias points [region A in Fig. 1(c)] of a Nb/AlO$_x$/Nb junction with a length of $L = 250$ μm for different applied magnetic fields. The flux values in units of Φ_0 calculated from the applied magnetic field are indicated.

to those described in Ref. 18. We want to stress that we used a different imaging procedure ("voltage imaging" instead of "current imaging;" see Ref. 33) and a more sensitive imaging technique in the present measurements. Two conditions have to be fulfilled to be able to image static properties, i.e., the critical current distribution of the junction, while the junction is biased in the dynamic state ($V \neq 0$): (1) The I-V curve must be nonhysteretic (McCumber like; see Fig. 4) where the critical current is almost suppressed. This means that the state of the junction is close to a minimum of the $I_c(H)$ pattern or a high magnetic field is present. This is different to the conditions for the imaging procedure described in Ref. 18. (2) The junction should be biased at $(I, V) \approx (0, 0)$ to avoid interaction with, for example, Fiske resonances. At these bias points the I-V curve is very sensitive to a beam-induced change of the critical current I_c as can be seen from Fig. 4.

Under these conditions the dominant effect of the electron beam heating is a change of the critical current $I_c = \int_0^L \int_0^W j_c(x, y) \sin \varphi(x, y) dx dy$. The Josephson current density is assumed to be uniform $j_c(x, y) \equiv j_c$ which can easily be checked by imaging the spatial distribution of the quasiparticle conductance of the junction.[33] The beam-induced change of the critical current density Δj_c is therefore independent of the beam position (x_0, y_0) inside the junction window. In the case of a weak perturbation (beam spot size $\ll L, W$) and if we further neglect nonlocal effects (see Ref. 18 and references therein) the change of the critical current is given by

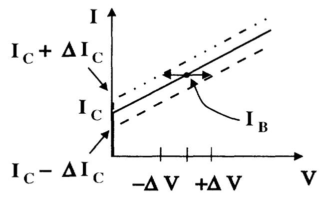

FIG. 4. Beam-induced change of the McCumber-like I-V characteristic close to the origin. The solid line represents an unperturbed I-V curve, whereas the dashed and the dashed-dotted lines represents two I-V curves perturbed with the electron beam.

$$\Delta I_c = \Delta j_c \sin \varphi(x_0, y_0) . \tag{3}$$

A positive and negative value is possible and has been observed experimentally [Figs. 3(a) and 3(b)] as well as in the numerical simulations as will be discussed below. The critical current of the irradiated junction $I_{c,\mathrm{irr}}$ is a function of the beam position (x_0, y_0): $I_{c,\mathrm{irr}} = I_c + \Delta I_c(x_0, y_0)$. As a consequence the I-V curve around the origin is shifted upwards or downwards (see Fig. 4). In a current-biased junction, in the limit of small perturbation, the voltage signal is therefore given by[29,33]

$$\Delta V(x_0, y_0) = -\left.\frac{\partial V}{\partial I}\right|_{I_B} \Delta I(x_0, y_0) . \tag{4}$$

$\partial V/\partial I$ describes the dynamic resistance of the junction. We have checked that the quasiparticle conductance was homogeneous for all junctions investigated by imaging the distribution of the quasiparticle conductance (for more details we refer to Ref. 33). $\Delta I(x_0, y_0)$ describes the change of the dc current in the heated area around the beam focus (x_0, y_0). According to the higher value of the dynamic resistance at the bias points $(I, V) \longrightarrow (0, 0)$ we have detected a relatively large signal (≈ 0.5 μV) in this range.

Increasing the bias current and reaching, for example, half of the asymptotic FFS voltage or the FFS, the structure of the line scans changed completely. A new approach to describe these patterns has to be used. In addition to a local change of j_c, a beam-induced increase of the quasiparticle losses α and of the surface losses β has to be taken into account. The increase of the losses inside the junction and the beam-induced perturbation of the fluxon nucleation and annihilation at the boundaries are now the dominant effects for the dynamic states with high fluxon velocity. A reduction of the average fluxon speed will reduce the average voltage V in a current-biased junction. The beam-induced change of the critical current I_c only modifies the I-V curve close to the origin. Therefore no contribution of the change of j_c was observed for bias points in regions B and C [see Fig. 1(c) and Figs. 5(a)–5(d), 6(a)–6(d), and 7(b), 7(c)].

The imaging of a pure Fiske mode is described in detail elsewhere.[25,29] In this case the line scans $-\Delta V(x_0, y_0)$ turned out to be proportional to the square of the time-averaged local ac magnetic field. Imaging a pure soliton-like mode, different patterns are obtained. The nucleation of a fluxon and also its collision with other fluxons or with the boundaries of the junction are related to an energy loss $\Delta\mathcal{H}$ which is proportional to the loss term α.[29,35,36] Due to the electron beam irradiation the losses are increased and the speed of the fluxon is reduced. Therefore, the voltage at the bias point I_B is

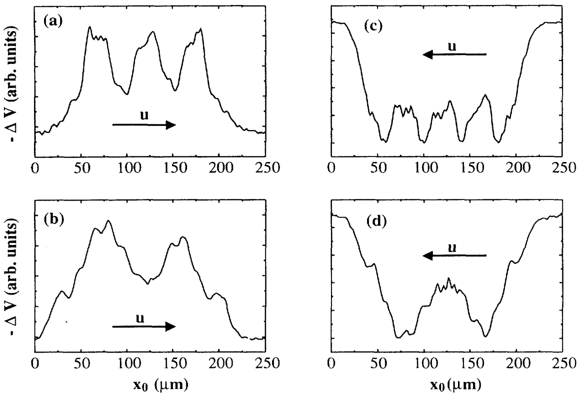

FIG. 5. Line scans $-\Delta V(x_0)$ of bias points in the intermediate range [region B in Fig. 1(c)] of a Nb/AlO$_x$/Nb junction with a length of $L = 250$ μm. The applied magnetic field was 0.3 mT corresponding to $6.7\Phi_0$ for all the line scans. The arrows show the direction of the fluxon motion. The bias current was increased from (a) to (b); (c) and (d) show the images obtained for reversed bias current.

shifted downwards and a beam-induced voltage signal $-\Delta V(x_0, y_0)$ is detected. In the case of the flux-flow mode both mechanisms have to be taken into account. First, we have a perturbation of the fluxon nucleation and annihilation at the boundaries. Second, the losses in the junction are increased, perturbing the fluxon motion as well as the cavity-mode excitations.

Biasing the junction in the intermediate range [area B in Fig. 1(c)] a complex dynamic behavior is expected.[9,37] The traveling fluxon chain, which can be considered as a traveling wave, interacts with reflected waves and cavity-mode excitations (due to the large impedance mismatch at the boundaries of the junction), especially for a low-damped junction as in our experiments. Due to the superposition of the traveling wave and the reflected waves a complex standing-wave pattern is formed and complex line scans are obtained [Figs. 5(a)–5(d) and 6(a); arrows labeled with u indicate the direction of the fluxon motion as obtained by the polarity of the applied magnetic field and the direction of the bias current; see also patterns of the ac electric field obtained by numerical simulations in Refs. 9, 37]. The main effect of the electron beam irradiation is a local increase of the losses and the line scans are proportional to the time-averaged ac magnetic field. Superimposed to the basic structure we observed, when biasing the junction close to a voltage of a Fiske-resonance, a fine structure [Figs. 5(b) and 5(d)] which is related to the order or the corresponding Fiske step. Such behavior was also found in in-line junctions [see for example Figs. 9(a) and 9(b) in Ref. 29].

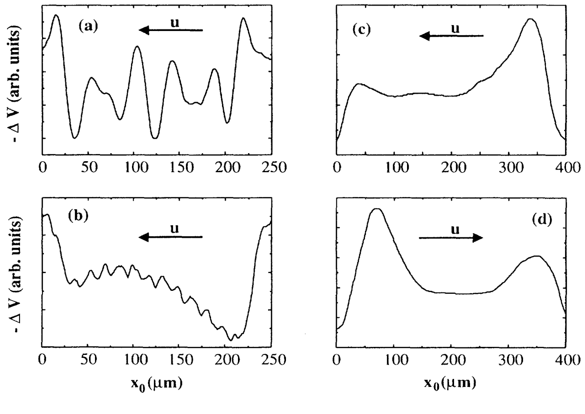

FIG. 6. Line scans $-\Delta V(x_0)$ of different states in different Nb/AlO$_x$/Nb junctions. The arrows show the direction of the fluxon motion. Part (a) shows a line scan in the intermediate range ($L = 250$ μm, $B = 0.26$ mT) and part (b) a line scan at the top of a FFS with low damping ($L = 250$ μm, $B = 0.3$ mT) and with reversed bias current. Parts (c) and (d) show line scans in a junction with $L = 400$ μm for similar bias points but with reversed fields $\mid B \mid= 0.41$ mT, respectively.

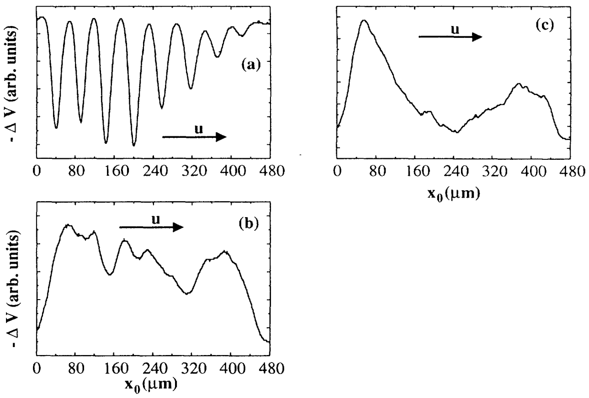

FIG. 7. Line scans $-\Delta V(x_0)$ of a Nb/NbO$_x$/Pb junction. Part (a) corresponds to region A in Fig. 1 (c), part (b) to region B, and part (c) to region C.

Biasing the junction at the FFS [regime C in Fig. 1(c)] the patterns changed again. Now the line scans show two pronounced maxima at the boundaries of the junction [Figs. 6(b) and 6(c)]. At the boundaries the electron-beam-induced increase of the damping perturbs the nucleation and the annihilation process of the fluxons. A decrease of the fluxon velocity in comparison with the unperturbed junction results in a voltage signal $-\Delta V(x_0) > 0$. The largest voltage signal is observed close to the boundary where the fluxons enter the junction. We proved this by reversing the direction of the fluxon propagation, either by reversing the polarity of the bias current or the orientation of the applied magnetic field. In the region near to the fluxon nucleation site the fluxons are accelerated to the ultimate velocity with which they move deeper inside the junction. An additional energy loss (due to the electron beam heating) in the acceleration area produces a substantial decrease of the fluxon time of flight through the junction, thereby giving a large voltage response. In contrast to the flux flow in in-line junctions [see for example Figs. 9(a) and 9(b) in Ref. 29], the fluxons experience a nearly homogeneous driving force over the whole length of the junction with an overlap geometry. After acceleration the fluxons propagate through the junction with a nearly constant velocity u (which is approaching $\bar{c}$ at the top of the FFS). Therefore, no decrease of the signal in the direction of the fluxon motion is observed. In addition, we observed a second, smaller maximum, at the boundary where the fluxons annihilate.

Maxima in the ac electric field and in the dc supercurrent at the boundary where the fluxons leave the junction were reported in the simulations of Refs. 9 and 37. Oscillations of the amplitude of the electric field are related to a corresponding variation of the fluxon speed and, hence, in this sample region a pronounced voltage signal is expected by perturbing the system with the electron beam.

The structure of our line scans in the middle of the junction depends on the damping of the system. In the case of higher damping—due to a higher temperature of the sample or due to a higher voltage and, hence frequency, at the bias point—no fine structure between the two maxima at the borders was observed. We detected a homogeneous signal in this part of the junction [see Figs. 6(c) and 6(d)] because of the strong coupling of the fluxons. For a lower damping cavity mode excitations—superimposed on the fluxon motion—occurred and a fine structure on the basic pattern [see Fig. 6(b)] was observed. The number of fine structure maxima is in excellent agreement with the order of the corresponding Fiske-mode number (see numerical simulations below). All results described above were obtained with $\mathrm{Nb/AlO}_x\mathrm{/Nb}$ junctions. Using the $\mathrm{Nb/NbO}_x\mathrm{/Pb}$ junction, the obtained patterns remained very similar, which can be seen in Figs. 7(a)–7(c).

Using the technique of LTSEM we were able to image different states in the flux-flow regime of long Josephson junctions. The basic structure of the observed patterns was independent of the size (of course, the junction must be sufficiently long) and of the materials forming the junction. In the following section we present a detailed numerical simulation of our measurements.

III. NUMERICAL SIMULATIONS

In this section we first present the mathematical model of the PSGE. Second, we model the LTSEM line scans of the multiple-fluxon regime in long Josephson junctions of the overlap geometry. The LTSEM signal generation model used in the present simulations is a combination of two alternative approaches used previously and based on the local change of the critical current density[18] and the local change of the dissipation (quasiparticle tunnel conductivity) induced by the electron beam. The latter approach has been introduced by Lachenmann *et al.*[29] and has recently been used for analytical and numerical investigations for single-fluxon dynamic states.[36]

A. Basic equation

The dynamics of a long Josephson junction is described by the PSGE with the spatial coordinate x normalized to λ_J and the time t normalized to the inverse plasma frequency ω_0^{-1}:

$$\varphi_{xx} - \varphi_{tt} - \sin\varphi = \alpha\varphi_t - \beta\varphi_{xxt} - \gamma \,, \qquad (5)$$

where $\varphi(x,t)$ is the phase difference between the superconducting electrodes of the junction. The subscripts denote the partial derivatives with respect to the indicated variables. The last term γ is the normalized bias current which acts as a homogeneous driving force on fluxons in the junction. For simplicity, in the following it is assumed that the surface current loss term $\beta(x) \equiv 0$. The spatially dependent function $\alpha = \alpha(x)$ can be considered as an effective damping term [for low fluxon velocities u it can be shown that $\alpha_{\text{eff}} \sim \alpha + \beta/3$ (Ref. 16)] including both the quasiparticle tunneling and the surface current losses. Under these assumptions Eq. (5) for an overlap junction has to be solved together with the boundary conditions

$$\varphi_x(0,t) = \varphi_x(l,t) = h \,. \qquad (6)$$

An analytical treatment of this problem requires a perturbation approach[15,16] based on exact solutions of the pure sine-Gordon equation ($\alpha, \beta, \gamma = 0$) or a numerical treatment.[9,15,34]

B. Signal generation modeling

In order to simulate the LTSEM response of a long Josephson junction, we use the PSGE (5) in the following form:

$$\varphi_{xx} - \varphi_{tt} = f(x)\sin\varphi + \alpha(x)\varphi_t - \gamma \,, \qquad (7)$$

where $f(x)$ accounts for the spatial variations of the critical current density and $\alpha(x)$ models the spatial dependence of the losses in the junction.

In the LTSEM experiment the electron beam produces a local heating of the junction around the beam position (x_0, y_0). Thereby, in the frame of an one-dimensional model, $\alpha(x)$ is locally increased and $f(x)$ is reduced. The electron beam perturbation is modeled by a localized "hot spot" placed at the point $x = x_0$ (measured in units of λ_J) and described by the following functions:

$$f(x) = 1 + \eta_1\,\delta(x - x_0) \,, \quad \alpha(x) = \alpha_0 g(x),$$

$$g(x) = 1 + \eta_2\,\delta(x - x_0). \qquad (8)$$

In the simulations the δ functions were approximated by the expression

$$\eta_{1,2}\delta(x - x_0) \approx \kappa_{1,2}\,\mathrm{sgn}(\eta_{1,2}) \left[1 - \tanh^2 \frac{2(x - x_0)}{\varepsilon_{1,2}}\right] , \qquad (9)$$

where $\varepsilon_{1,2}\kappa_{1,2} = \eta_{1,2}$. The local decrease of $f(x)$ and the increase of $\alpha(x)$ corresponds to $\eta_1 < 0$ and $\eta_2 > 0$, respectively ($\varepsilon_{1,2} > 0$).

In order to model the electron beam scanning procedure we calculate the time-averaged voltage across the Josephson junction as a function of x_0. This algorithm accounts for the experimental situation since the period of the fluxon oscillations is much shorter than the characteristic times of scanning and modulating of the electron beam.[29]

We numerically integrated Eq. (7) with boundary conditions (6). The simulations are performed with a normalized junction length $l = 10$ and a dissipation coefficient $\alpha_0 = 0.1$. The calculated average voltage $\tilde{V}$ is normalized to the voltage at the first Fiske step $\tilde{V}_{\rm FS1} = \pi/\ell$ in normalized units. The details of the simulations can be found elsewhere.[36] The LTSEM line scans are simulated in form of the dependence $-\Delta\tilde{V}(x_0)$ at several bias points on the I-V curve. The size of the heated spot $\mid \kappa_{1,2} \mid = \epsilon_{1,2} = 0.3$ used in our simulations corresponds to an estimated value of the junction area heated by the electron beam in the experiment.

C. Results and discussion

Figure 8 shows the numerically calculated current-voltage characteristic for the normalized magnetic field $h = 5$ without the beam-induced hot spot $[f(x) = g(x) = 1]$. The simulations were performed for both increasing and decreasing bias current.

Figures 9(a)–9(d) show the calculated voltage response $-\Delta\tilde{V}(x_0)$ obtained for different bias points (marked by capital letters K, L, M, and N in Fig. 8). Note that the voltage response is presented here in absolute units and is not inverted as in the experimental line scan. Scans shown by solid lines in Fig. 9 have been simulated with $\eta_1 = -0.09$ and $\eta_2 = 0.09$. In order to separate the influence of the terms with $f(x)$ and $\alpha(x)$ on the calculated line scans, two scans [shown by dashed lines in Figs. 9(a), 9(d)] have been performed with $\eta_1 = 0$ and $\eta_2 = 0.09$.

Multiple-fluxon states in a long Josephson junction are generated in a sufficiently large dc magnetic field, in normalized units $h > 2$ [see Eq. (6)]. In this case fluxons penetrate into the junction and the normalized spacing between them becomes $\xi \approx 2\pi/h$. The average number of fluxons simultaneously present in the junction is

$$N_f \approx \frac{\ell}{\xi} . \qquad (10)$$

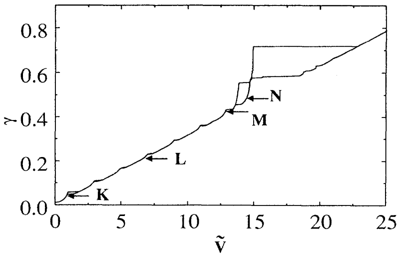

FIG. 8. Numerically calculated current-voltage characteristics of a long overlap Josephson junction with the normalized length $\ell = 10$ and the dissipation coefficient $\alpha = 0.1$ without electron beam perturbation $[f(x) = g(x) = 1]$ in the magnetic field $h = 5$. Current γ and voltage $\tilde{V}$ are measured in normalized units.

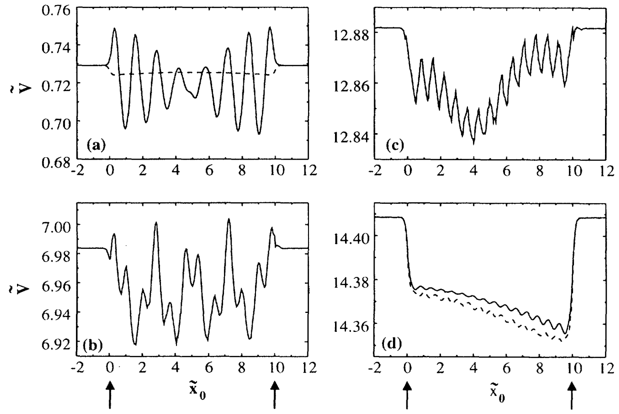

FIG. 9. Change of the average voltage as a function of the heated spot position $\tilde{x}_0$ (measured in units of λ_J) for the different bias points of the $\gamma\tilde{V}$ curve shown in Fig. 8: (a) point K, (b) point L, (c) point M, (d) point N. Arrows indicate the junction boundaries at $x_0 = 0$ and $x_0 = 10$. The dashed lines in (a) and (d) correspond to simulations neglecting the electron-beam-induced change of the critical Josephson current density.

If a sufficiently large bias current γ is applied, the whole fluxon chain moves along the junction with the velocity u close to the Swihart velocity $\bar{c}$. The fluxon motion is detected experimentally by observing the FFS in the I-V characteristics. The step appears at the normalized voltage (in units of $V_{\rm FS1}$)

$$\tilde{V} = \tilde{V}_{\rm FFS} \approx 2N_f . \qquad (11)$$

In the calculated I-V characteristics (Fig. 8) the FFS is split into two closely positioned Fiske steps at $\tilde{V} \approx 14$ and $\tilde{V} \approx 15$. This voltage is in a fairly good agreement with Eq. (11) which yields $\tilde{V}_{\rm FF} = 15.9$. The reason for the splitting of the FFS into Fiske steps can be understood as follows. In the flux-flow mode at $h > 0$ [note the minus sign in front of γ in Eq. (5)] the fluxons move from the boundary $x = \ell$ towards the other boundary $x = 0$. When they reach the boundary $x = 0$ a reflected wave appears, which yields cavity resonances (Fiske steps) over the length of the junction. The whole I-V curve is discretized into Fiske steps of small amplitudes with a voltage spacing of about 1. Fiske steps appear since the damping in the junction is not sufficiently large and the attenuation criterion for the reflected wave $\ell/\alpha \gg 1$ is not satisfied.[9]

The line scan of the dynamic state on the FFS [Figs. 9(c), 9(d)] displays the asymmetry which has also been observed experimentally. In Fig. 9(d) the larger signal appears at the right side of the junction where the fluxons enter. Additional simulations indicated that the reversal of the polarity of the magnetic field h or the bias current γ (which reverses the direction of the flux flow) also reverses the asymmetry of the voltage response. This asymmetry can be qualitatively understood from the analytically calculated dependence of the LTSEM voltage signal on the fluxon velocity u.[36] After fluxons enter the junction at one of its boundaries they get accelerated to almost Swihart velocity. This acceleration process takes place on some spatial interval[9] starting from the boundary where their velocity u is lower than in the rest of the junction. The velocity change averaged along the whole junction can be calculated as[36]

$$\Delta\bar{u} = \frac{\eta_2}{L}u(1-u^2)\ . \tag{12}$$

Thus, in the relativistic limit $u \to 1$ the LTSEM response decreases with increasing the fluxon velocity u.

The high-velocity voltage response displays the number of maxima N_n [minima in the absolute voltage scale shown in Fig. 9(d)] being equal to the order of the Fiske step n in agreement with the experimental data. For the 15th Fiske step response shown in Fig. 9(d) we find $n = 15$.

Contrary to the FFS pictures, the line scans obtained at the lower voltages display the number of maxima, N_m, being approximately equal to the number of fluxons, N_f (for the FFS the number of maxima is approximately equal to $2N_f$) in the junction. With $h = 5$, Eq. (10) yields $N_f \approx 7.9$, and the line scan for the lowest bias point [Fig. 9(a)] displays $N_m = 7$ (or, even, $N_m = 7\frac{1}{2}$ since the central maximum is of split in two). For $h = 4$ we find $N_f \approx 6.4$, and the line scan displays $N_m \approx 6$.

In the intermediate voltage region [region (B) in Fig. 1(c)] the voltage response shows a complicated crossover from the low-voltage to the high-voltage response. We found similar patterns in our experimental and numerical investigations [compare Fig. 5(a), Fig. 7(b) with Fig. 9(b), also Fig. 5 with Fig. 9(c)]. However, a detailed quantitative comparison between the simulations and the experiment seems to be difficult.

As already discussed above in Sec. II, the fact that the number of periods of the low-voltage response is equal to the number N_f of fluxons in the junction can be naturally understood from the earlier LTSEM studies of *static vortex states* in Josephson junctions.[18] In such experiments, the electron beam scanning across the junction leads to the periodic modulation of its critical current I_c with the number of periods being equal to the number of vortices (fluxons) present in the junction. Obviously, the change in the critical current I_c influences the low-voltage part of the I-V characteristics, where the increase of I_c should decrease the voltage for a given bias current.

In order to separate the contribution of the critical current modulation $f(x)$ from that of the dissipative term $\alpha(x)$, we have calculated also the voltage response with $\eta_1 = 0$. Such a purely dissipative perturbation line scan is shown by the dashed lines in Figs. 9(a) and 9(d). One can see that the high-voltage dynamic state (FFS) response shown in Fig. 9(d) displays minor changes, and that the number of maxima, N_m, remains unchanged. Thus, the dissipative-term perturbation plays the major role in this case. However, the low-voltage response [Fig. 9(a)] shows a drastic change, and the oscillations with $N_m \sim N_f$ periods disappear. We conclude that the electron-beam-induced dissipative-term perturbation alone cannot explain the experimental LTSEM line scans obtained at low voltages. In this case the proper signal generation model must include the perturbation which interacts with static fluxons, i.e., the beam-induced change of the critical current and/or the inductive term φ_{xx}.

IV. SUMMARY

We have performed spatially resolved investigations of the flux-flow behavior in different types of long overlap Josephson junctions. For our junctions with low damping we can divide the fluxon behavior into three different regimes. First, for bias points close to $(I, V) \to (0,0)$ the observed patterns show the static distribution of the Josephson current in the presence of an external magnetic field. The number of signal periods is equal to the number of fluxons inside the junction. It is necessary to stress that the LTSEM imaging of static junction properties in a state with $V \neq 0$ is only possible under specific conditions (a nonhysteretic I-V curve and a bias point close to the origin). A second, intermediate range $0 < V < V_{\rm FFS}$ shows a complicated behavior, due to an interaction of the traveling fluxon chain with the reflected wave and the cavity excitations. The observed fine structure is a clear indication that in this intermediate region and for a system with low damping a strong interaction of the fluxon chain with cavity resonances takes place. In the third region, we deal with the relativistic limit, where the fluxon velocity u approaches the Swihart velocity $\bar{c}$. Here we have observed additional maxima at the borders of the junctions. These maxima are due to a change of the energetic conditions for a fluxon entering or leaving the junction. For low damping (low step voltage $V_{\rm FFS}$) we have observed a fine structure which is related to the order n of the pumped Fiske mode $V_{\rm FFS} \approx V_{{\rm FS},n}$. For higher damping this fine structure disappeared and the patterns were dominated by the perturbation of the fluxons at the boundaries. For understanding these results an electron-beam-induced change of the losses and a change of the critical current have to be taken into account, depending on the bias point.

Theoretical models for describing the experimental LTSEM measurements of the multiple-fluxon dynamic states in long Josephson junctions are examined by numerical simulations. Two types of perturbations which contribute to the LTSEM signal are examined, namely, the local perturbation of the damping term α and that of the critical current density j_c in the junction. In agreement with the experiment, at high fluxon velocities in both cases the voltage response is found to be spatially asymmetric, with the periodic modulation corresponding to the number of the Fiske step. The asymmetry of the calculated line scans reverses with the reversal of the direction of the fluxon motion. At low fluxon velocities, the model which includes only the α-term perturbation is unable to explain the experimental data. However, the model which includes both the α- and j_c-type perturbations shows good qualitative agreement with experiment, displaying the spatial voltage response with the number of maxima being equal to the number of fluxons in the junction.

ACKNOWLEDGMENTS

We thank B. A. Malomed for valuable discussions. We gratefully acknowledge the support of this work by the Deutsche Forschungsgemeinschaft. A.V.U. thanks the Alexander von Humboldt Stiftung for support during the initial part of this work.

---

[1] B. D. Josephson, Phys. Lett. **1**, 251 (1962).

[2] A. Barone and G. Paterno, *Physics and Applications of the Josephson Effect* (John Wiley, New York, 1982).

[3] K. K. Likharev, *Dynamics of Josephson Junctions and Circuits* (Gordon and Breach, New York, 1986).

[4] J. Niemeyer, J. H. Hinken, and R. L. Kautz, Appl. Phys. Lett. **45**, 478 (1984).

[5] R. L. Kautz, C. A. Hamilton, and F. L. Lloyd, IEEE Trans. Magn. **MAG-23**, 883 (1987).

[6] M. B. Ketchen, IEEE Trans. Magn. **MAG-17**, 387 (1981).

[7] J. Clarke, in *The New Superconducting Electronics*, edited by H. Weinstock and R. W. Ralston (Kluwer Academic, Dordrecht, 1993), p. 123.

[8] J. R. Tucker and M. J. Feldman, Rev. Mod. Phys. **57**, 1055 (1985).

[9] T. Nagatsuma, K. Enpuku, F. Irie, and K. Yoshida, J. Appl. Phys. **54**, 3302 (1983); **56**, 3284 (1984); T. Nagatsuma, K. Enpuku, K. Sueoka, K. Yoshida, and F. Irie, *ibid.* **58**, 3302 (1985).

[10] A. V. Ustinov, T. Doderer, R. P. Huebener, J. Mygind, V. A. Oboznov, and N. F. Pedersen, IEEE Trans. Appl. Supercond. **AS-3**, 2287 (1993).

[11] Y. Zhang, D. Winkler, and T. Claeson, Appl. Phys. Lett. **62**, 3195 (1993).

[12] V. P. Koshelets, A. V. Shchukin, S. V. Shitov, and L. V. Filipenko, IEEE Trans. Appl. Supercond. **AS-3**, 2524 (1993).

[13] N. F. Pedersen, IEEE Trans. Magn. **MAG-27**, 3328 (1991).

[14] K. K. Likharev, Supercond. Sci. Technol. **3**, 325 (1990).

[15] R. D. Parmentier, in *The New Superconducting Electronics*, edited by H. Weinstock and R. W. Ralston (Kluwer Academic, Dordrecht, 1993), p. 221.

[16] D. W. McLaughlin and A. C. Scott, Phys. Rev. A **18**, 1652 (1978).

[17] S. Kiryu, S. Kohjiro, A. Shoji, S. Kodaira, J. Inantani, and S. Sato, IEEE Trans. Appl. Supercond. **AS-3**, 2528 (1993).

[18] J. Bosch, R. Gross, M. Koyanagi, and R. P. Huebener, Phys. Rev. Lett. **54**, 1448 (1985); J. Low Temp. Phys. **68**, 245 (1987).

[19] J. Mannhart, J. Bosch, R. Gross, and R. P. Huebener, Phys. Rev. B **35**, 5267 (1987).

[20] J. Mannhart, J. Bosch, R. Gross, and R. P. Huebener, J. Low Temp. Phys. **70**, 459 (1988).

[21] J. R. Lhota, M. Scheuermann, P. K. Kuo, and J. T. Chen, Appl. Phys. Lett. **44**, 255 (1983).

[22] S. Meepagala, J. T. Chen, and J.-J. Chang, Phys. Rev. B **36**, 809 (1987).

[23] T. Doderer, D. Quenter, B. Mayer, C. A. Krulle, A. V. Ustinov, R. P. Huebener, J. Niemeyer, R. Fromknecht, R. Pöpel, U. Klein, P. Dammschneider, and J. H. Hinken, in *Nonlinear Superconductive Electronics and Josephson Devices*, edited by X. Costabile, S. Pagano, N. F. Pedersen, and M. Russo (Plenum, New York, 1991), p. 353.

[24] C. A. Krulle, T. Doderer, D. Quenter, R. P. Huebener, R. Pöpel, and J. Niemeyer, Appl. Phys. Lett. **59**, 3042 (1991).

[25] B. Mayer, T. Doderer, R. P. Huebener, and A. V. Ustinov, Phys. Rev. B **44**, 12 463 (1991).

[26] A. V. Ustinov, T. Doderer, R. P. Huebener, B. Mayer, and V. A. Oboznov, Europhys. Lett. **19**, 63 (1992), A. V. Ustinov, T. Doderer, R. P. Huebener, N. F. Pedersen, B. Mayer, and V. A. Oboznov, Phys. Rev. Lett. **69**, 1815 (1992).

[27] A. V. Ustinov, T. Doderer, B. Mayer, R. P. Huebener, A. A. Golubov, and V. A. Oboznov, Phys. Rev. B **47**, 944 (1993).

[28] T. Doderer, S. G. Lachenmann, A. V. Ustinov, D. Quenter, and R. P. Huebener, Phys. Scr. T **49**, 172 (1993).

[29] S. G. Lachenmann, T. Doderer, R. P. Huebener, D. Quenter, J. Niemeyer, and R. Pöpel, Phys. Rev. B **48**, 3295 (1993).

[30] D. Quenter, S. Stehle, T. Doderer, C. A. Krülle, R. P. Huebener, F. Müller, J. Niemeyer, R. Pöpel, T. Weimann, R. Ruby, and A. T. Barfknecht, Appl. Phys. Lett. **63**, 2135 (1993).

[31] S. G. Lachenmann, G. Filatrella, T. Doderer, J. C. Fernandez, and R. P. Huebener, Phys. Rev. B **48**, 16 623 (1993).

[32] M. Cirillo, U. Gambardella, and S. Pace, Phys. Scr. **38**, 600 (1988).

[33] R. P. Huebener, in *Advances in Electronics and Electron Physics*, edited by P. W. Hawkes (Academic, New York, 1988), Vol. 70, pp. 1–75.

[34] P. S. Lomdahl, O. H. Soerensen, and P. L. Christiansen, Phys. Rev. B **25**, 5737 (1982).

[35] N. F. Pedersen, M. R. Samuelsen, and D. Welner, Phys. Rev. B **30**, 4057 (1984).

[36] B. A. Malomed and A. V. Ustinov, Phys. Rev. B **49**, 13 024 (1994).

[37] Y. Zhang, Ph.D. thesis, Chalmers University of Technology, Göteborg, 1993.

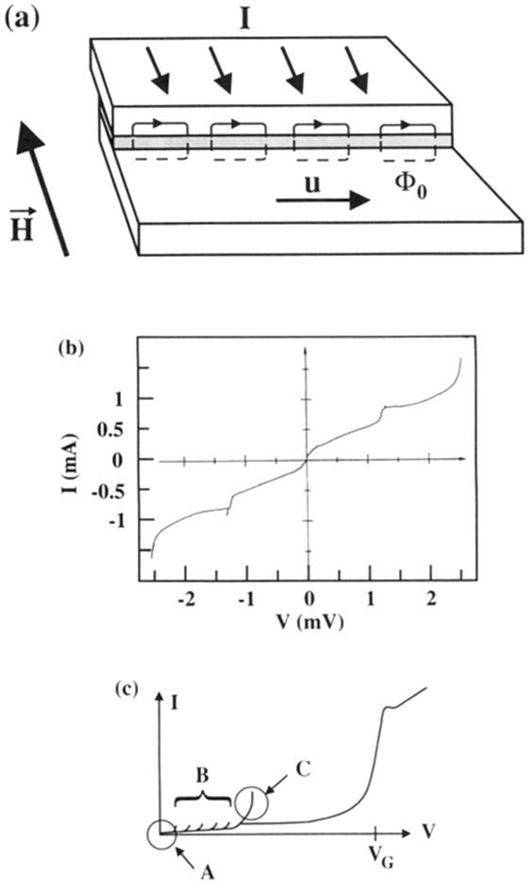

FIG. 1. Flux flow in overlap Josephon junctions. Part (a) shows a schematic drawing of a fluxon chain traveling through the junction with the speed u driven by the bias current I. $\vec{H}$ indicates the orientation of the applied magnetic field. Part (b) represents an experimental I-V curve in a Josephson junction of $L = 400$ μm with an external field of 0.81 mT. (c) shows a schematic I-V curve; A, B, and C indicate different regions of the flux-flow regime; V_G denotes the gap voltage.